

Twisty Takens: A Geometric Characterization of Good Observations on Dense Trajectories

Boyan Xu^{*}, Christopher J. Tralie[†], Alice Antia[‡], Michael Lin[§], Jose A. Perea[¶]

February 20, 2024

Abstract

In nonlinear time series analysis and dynamical systems theory, Takens' embedding theorem states that the sliding window embedding of a generic observation along trajectories in a state space, recovers the region traversed by the dynamics. This can be used, for instance, to show that sliding window embeddings of periodic signals recover topological loops, and that sliding window embeddings of quasiperiodic signals recover high-dimensional torii. However, in spite of these motivating examples, Takens' theorem does not in general prescribe how to choose such an observation function given particular dynamics in a state space. In this work, we state conditions on observation functions defined on compact Riemannian manifolds, that lead to successful reconstructions for particular dynamics. We apply our theory and construct families of time series whose sliding window embeddings trace tori, Klein bottles, spheres, and projective planes. This greatly enriches the set of examples of time series known to concentrate on various shapes via sliding window embeddings, and will hopefully help other researchers in identifying them in naturally occurring phenomena. We also present numerical experiments showing how to recover low dimensional representations of the underlying dynamics on state space, by using the persistent cohomology of sliding window embeddings and Eilenberg-MacLane (i.e., circular and real projective) coordinates.

Acknowledgments

C.J. Tralie was partially supported by an NSF big data grant DKA-1447491 and an NSF Research Training Grant NSF-DMS 1045133; J.A. Perea was partially supported by the NSF (DMS-1622301) and DARPA (HR0011-16-2-003); all authors were supported by the NSF under Grant No. DMS-1439786 while in residence at the Institute for Computational and Experimental Research in Mathematics in Providence, RI, during the Summer at ICERM 2017 program on Topological Data Analysis.

1 Introduction

The *delay coordinate mapping*, or *sliding window embedding* [35, 25, 20, 7], posits a time series as a sequence of observations made along trajectories in a hidden state space. Under this scheme, a one

^{*}Department of Mathematics, University of California at Berkeley, CA, USA.

[†]Department of Mathematics, Duke University, NC, USA.

[‡]Carleton College, MN, USA.

[§]Princeton University, NJ, USA.

[¶]Department of Computational Mathematics, Science and Engineering & Department of Mathematics Michigan State University, MI, USA.

dimensional time series, which could otherwise be analyzed with more traditional linear analysis techniques such as ARMA and Fourier/Wavelet analysis, is instead turned into a geometric object via a vector of samples of the time series, which moves along the signal (Equation 1). The shape of this geometric object provides information about the system under study. Periodic processes, for example, map to points which concentrate on a topological loop. Sliding window embeddings have been used in this context, for example, to analyze ECG signals of a beating heart [34, 32], to detect chatter in mechanical systems [21], to quantify repetitive motions in human activities [14, 40], to discover periodicity in gene expression during circadian rhythms [30], and to detect wheezing in audio signals [13]. In addition to loops, torus shapes often show up during “quasiperiodicity,” which is a state of near-chaos. Sliding window embeddings have witnessed this torus shape in such applications as vocal fold anomalies [19], horse whinnies [4], neural networks [24], and oscillating cylinder flow [17]. Certain time series even concentrate on fractals after a sliding window embedding [35, 9]. Sliding window embeddings have also been used as a tool for shape analysis more generally even when an underlying model for the dynamics is unknown, such as in music structure analysis [3, 33].

The main theory motivating the use of sliding window embeddings in all of these applications is Takens’ delay embedding [35] theorem, which is stated as follows:

Theorem 1.1 (Takens’ embedding theorem [35]). *Let M be a compact manifold of dimension m . For pairs (X, G) , X a smooth vector field and G a smooth function on M , it is a generic property that $\Psi : M \rightarrow \mathbb{R}^{2m+1}$ defined by $\Psi(p) = (G(p), G(\psi_1(p)), G(\psi_2(p)), \dots, G(\psi_{2m}(p)))$ is an embedding.*

A “random” choice of X and G makes the delay coordinate mapping Ψ a smooth embedding. Thus, remarkably, the state space M of a dynamical system may in general be reconstructed from a single generic observation function G ¹, which gives rise to a 1D time series. However, in practice, Takens’ result is ill-suited for computational purposes because it does not provide an explicit characterization of “genericity”. In this work, we extend Takens’ embedding theory to include high-dimensional delay coordinate mappings and provide a geometric characterization of observations which yield delay coordinate embeddings, given a particular flow on a manifold. Our main theoretical result for general compact manifolds is stated in Theorem 4.1 in Section 4. We provide several examples in Section 3 which satisfy the conditions of our theorem, and we explore a special case in Section 5 in which Fourier bases can be used to construct observation functions².

2 Background

In this section, we provide a more detailed overview of several concepts utilized in this work, including sliding window embeddings, persistent (co)homology, and Eilenberg-MacLane coordinates. The latter two tools will be used to empirically validate that our sliding window embeddings recover our chosen state space and the underlying dynamics.

2.1 Sliding Window Embeddings

We express a time series $g(t)$ as an observation G along a dense trajectory γ on a manifold M , i.e.

$$g(t) = G(\gamma(t))$$

¹Some texts refer to this as an “observable.”

²The code to generate all figures in this manuscript can be found at <http://www.github.com/ctralie/TwistyTakens>

for $\gamma : \mathbb{R} \rightarrow M$ and $G : M \rightarrow \mathbb{R}$. We compute the *sliding window* of g as

$$\text{SW}_\tau^N g(t) := \begin{bmatrix} g(t) \\ g(t + \tau) \\ g(t + 2\tau) \\ \vdots \\ g(t + N\tau) \end{bmatrix} \in \mathbb{R}^{N+1} \quad (1)$$

where $N \in \mathbb{N}$ is the number of delays, $\tau > 0$ is the delay time, and $N\tau$ is the window length.

We interpret the sliding window $\text{SW}_\tau^N g(t)$ as the evaluation of the Takens map Ψ in Theorem 1.1 above on an integral curve $\psi_t(p)$ of a vector field X through a point $p \in M$. For if $N = 2 \cdot \dim M$ and $\gamma(t) = \psi_t(p)$, then

$$\text{SW}_\tau^N g(t) = \Psi(\psi_t(p)).$$

For sufficiently large N and small τ , $\text{SW}_\tau^N g(t)$ densely “traces” the embedding $\Psi(M)$ for appropriate choice of observation G and vector field X .

When g is a periodic function with frequency $\omega \in \mathbb{R}$, it readily follows that the sliding window embedding $\text{SW}_\tau^N g(t)$ traces a closed curve in \mathbb{R}^{N+1} . The shape of this curve is closely related to the choice of parameters N and τ , and their relation to ω [31]. In particular, if τ and N are chosen so that N is large enough and $N\tau\omega \approx 1$, then the image of $\text{SW}_\tau^N g$ is in fact a topological circle in \mathbb{R}^{N+1} , whose shape is tightly controlled by the Fourier coefficients of g . In other words, the periodic nature of g — a spectral property — is reflected in the circularity of its sliding window, a topological feature. Quasiperiodicity is another spectral notion with a clear geometric/topological counterpart. Indeed, let $1, \omega_1, \dots, \omega_n \in \mathbb{R}$ be linearly independent over the rational numbers. We say that $f : \mathbb{R} \rightarrow \mathbb{R}$ is quasiperiodic with frequencies $\omega_1, \dots, \omega_n$, if it can be written as $f(t) = F(t, \dots, t)$ for some function $F : \mathbb{R}^n \rightarrow \mathbb{R}$ whose j -th marginals $f_j(t) = F(t_1, \dots, t_{j-1}, t, t_{j+1}, \dots, t_n)$ are periodic with frequency ω_j . In this case, and for appropriate N and τ , the set $\text{SW}_\tau^N f(\mathbb{Z})$ is dense in an n -dimensional torus embedded in \mathbb{R}^{N+1} [27, 15].

2.2 Koopman spectra

We now review another relevant tool that goes along with sliding window embeddings. For positive flow time $t > 0$, the flow ψ_t of a vector field X on a compact manifold M defines a diffeomorphism $\psi_t : M \rightarrow M$. Then the composition map U^t , or Koopman operator [22, 7, 23] given by

$$U^t G = G \circ \psi_t,$$

is a linear operator on the space of observation functions on M . The coordinates of the delay mapping are thus iterated applications of U^t on an observation G .

For certain classes of dynamical systems, the Koopman operator possesses a discrete spectrum and yields a linear expansion

$$G = \sum_{k=0}^{\infty} G_k \varphi_k$$

where φ_k are eigenfunctions of U^t and G_k are *Koopman modes*. For such systems one “lifts” the dynamics on the state space to an evolution of observables. For a more comprehensive overview of Koopman theory and its applications, please refer to [1].

We will see in Section 5 that a high-dimensional delay mapping essentially recovers the Koopman modes of an observation function. We therefore characterize delay embedding observations in terms of spectral decomposition properties. We examine a special case with a Fourier basis for the

Koopman operator on the Torus and Klein bottle, and show via our main Theorem 4.1 what is needed of these coefficients.

2.3 Persistent Homology

In practice we evaluate the sliding window $SW_\tau^N g(t)$ at a finite set of evenly sampled time points $t_1 < \dots < t_J$. This results in a discrete collection of J vectors, referred to as a “sliding window point cloud”. The topology of a point cloud with J points is trivial; it consists of J connected components and lacks any other topological features (loops, voids, etc). However, if we use a *simplicial complex* (a discrete object) to approximate the underlying space from which the point cloud is sampled, then we can estimate the underlying topology via combinatorial means. A simplicial complex on a set V of vertices (e.g., a sliding window point cloud) is a collection K of nonempty subsets $\sigma \subset V$, so that if $\emptyset \neq \tau \subset \sigma \in K$, then $\tau \in K$. As an example, suppose we seek a simplicial complex with topology reflecting that of the unit circle S^1 . Starting with the set $V = \{a, b, c\}$ of vertices, we let $K = \{a, b, c, \{a, b\}, \{b, c\}, \{a, c\}\}$ be the simplicial complex containing 3 edges between every pair of vertices. Like S^1 , K has one connected component, one loop which bounds an empty space, and no higher dimensional features (voids, etc).

So far, our description of simplicial complexes has been purely combinatorial/topological, but one can use geometry to inform their construction. An early scheme in Euclidean space is the alpha complex [12], constructed as a family of subcomplexes of Delaunay triangulations at different scales. An even simpler construction, which works in any metric space, is the so-called “Vietoris-Rips” complex at scale $\alpha \geq 0$, denoted $R_\alpha(V)$. It is comprised of the finite subsets of V which have diameter less than α . Choosing the “appropriate” scale is ill-posed. For instance, Figure 1 shows a point cloud in \mathbb{R}^2 for which it is impossible to choose an appropriate scale at which the simplicial complex contains the two empty loops that are present in the original shape.

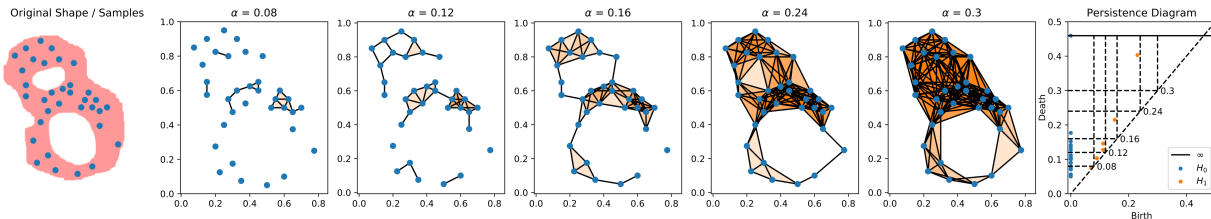


Figure 1: An example of the Rips filtration on a point cloud sampled from a thickened figure eight. The Rips complex is shown at different scales, the values of α , producing the persistence diagram on the right.

Specifically, $R_{0.16}(V)$ contains the upper loop, but not the lower loop, and $R_{0.24}(V)$ contains the lower loop, but the upper loop is no longer empty. In fact, it is impossible to choose an α in which both loops are present and empty in $R_\alpha(V)$ in this example. However, we can still summarize the multiscale topological information of any point cloud by performing a *filtration* of the complex. That is, we evaluate $R_\alpha(V)$ as α varies continuously from 0 to some maximum value, so that $R_{\alpha_1}(V) \subset R_{\alpha_2}(V)$ if $\alpha_1 \leq \alpha_2$. Throughout this process we keep track of topological features as they appear, or are “born,” and as they are filled in, or “die”. For each such *homology class*, we can produce a point in a scatter plot, known as the *persistence diagram* of the filtration, with birth time on the x -axis and death time on the y -axis. Figure 1 shows a persistence diagram associated with our running example³. Intuitively, points further from the diagonal correspond to

³We compute persistence diagrams for all examples in this paper using the Python interface to “Ripser” [2, 36]

larger topological features which “persist” (stay alive) over longer intervals, and points closer to the diagram correspond to small, “noisy” features which are often artifacts of sampling (e.g. the square and pentagon loop that exist at $\alpha = 0.12$).

For completeness, we extend the above explanation with a brief rigorous presentation. For a more comprehensive treatment, please refer to [10, 11, 5, 16, 28]. Let (Γ, \preceq) be a partially ordered set. A Γ -filtered simplicial complex is a collection $\mathcal{K} = \{K_\alpha\}_{\alpha \in \Gamma}$ of simplicial complexes, so that $K_\alpha \subset K_{\alpha'}$ for every $\alpha \preceq \alpha' \in \Gamma$. The typical examples for point cloud data are the Rips filtration, as we mentioned, and the Čech filtration motivated by the nerve lemma [18]. Specifically, let L be a finite subset of a metric space (\mathbb{M}, \mathbf{d}) . The Rips filtration of L is the \mathbb{R} -filtered simplicial complex $\mathcal{R}(L) = \{R_\alpha(L)\}_{\alpha \in \mathbb{R}}$. Similarly, for $\ell \in L$ let

$$B_\alpha(\ell) = \{b \in \mathbb{M} : \mathbf{d}(b, \ell) < \alpha\} \quad \text{and} \quad \mathcal{B}_\alpha = \{B_\alpha(\ell) : \ell \in L\}.$$

The Čech complex $\check{C}_\alpha(L)$ is defined as the nerve of \mathcal{B}_α ; that is $\check{C}_\alpha(L) = \mathcal{N}(\mathcal{B}_\alpha)$ where

$$\sigma \in \mathcal{N}(\mathcal{B}_\alpha) \quad \text{if and only if} \quad \bigcap_{\ell \in \sigma} B_\alpha(\ell) \neq \emptyset$$

Hence $\check{C}(L) = \{\check{C}_\alpha\}_{\alpha \in \mathbb{R}}$ is an \mathbb{R} -filtered simplicial complex, and $R_\alpha(L) \subset \check{C}_\alpha(L) \subset R_{2\alpha}(L)$ for all $\alpha \in \mathbb{R}$.

The persistent homology (resp. cohomology) of a filtered complex $\mathcal{K} = \{K_\alpha\}_{\alpha \in \Gamma}$, with coefficients in a field \mathbb{F} , are defined, respectively, as

$$PH_n(\mathcal{K}; \mathbb{F}) := \bigoplus_{\alpha \in \Gamma} H_n(K_\alpha; \mathbb{F}) \quad \text{and} \quad PH^n(\mathcal{K}; \mathbb{F}) := \bigoplus_{\alpha \in \Gamma} H^n(K_\alpha; \mathbb{F})$$

Let $\iota_{\alpha, \alpha'} : H_n(K_\alpha; \mathbb{F}) \rightarrow H_n(K_{\alpha'}; \mathbb{F})$ and $j^{\alpha', \alpha} : H^n(K_{\alpha'}; \mathbb{F}) \rightarrow H^n(K_\alpha; \mathbb{F})$ be the \mathbb{F} -linear maps induced by the inclusion $K_\alpha \subset K_{\alpha'}$, $\alpha \preceq \alpha'$. A persistent homology (resp. cohomology) class is an element $\oplus \nu_\alpha \in PH_n(\mathcal{K}; \mathbb{F})$ (resp. $\oplus \mu^\alpha \in PH^n(\mathcal{K}; \mathbb{F})$) so that $\iota_{\alpha, \alpha'}(\nu_\alpha) = \nu_{\alpha'}$ (resp. $j^{\alpha', \alpha}(\mu^{\alpha'}) = \mu^\alpha$) for every $\alpha \preceq \alpha'$.

When $\Gamma = \mathbb{R}$, a theorem of Crawley-Boevey [6] contends that if each $H_n(K_\alpha; \mathbb{F})$ is finite-dimensional (also known in the literature as being pointwise-finite) then one can choose bases S^α for each $H_n(K_\alpha; \mathbb{F})$, satisfying the following compatibility condition:

1. $\iota_{\alpha, \alpha'}(S^\alpha) \subset (S^{\alpha'} \cup \{0\})$ for every $\alpha \preceq \alpha'$.
2. If $\iota_{\alpha, \alpha'}(\mathbf{v}_j^\alpha) = \iota_{\alpha, \alpha'}(\mathbf{v}_k^\alpha)$ and $j \neq k$, then $\iota_{\alpha, \alpha'}(\mathbf{v}_j^\alpha) = 0$.

The set $S = \bigcup_{\alpha \in \mathbb{R}} S^\alpha$ admits a partial order \preceq given by $S^\alpha \ni \mathbf{v} \preceq \mathbf{v}' \in S^{\alpha'}$ if and only if $\alpha \leq \alpha'$ and $\iota_{\alpha, \alpha'}(\mathbf{v}) = \mathbf{v}'$. The maximal chains in (S, \preceq) are the persistent homology classes. To each maximal chain $\mathcal{C} \subset S$ one can associated the point $(b_\mathcal{C}, d_\mathcal{C}) \in [-\infty, \infty] \times [-\infty, \infty]$ defined by

$$b_\mathcal{C} = \inf\{\alpha \in \mathbb{R} : S^\alpha \cap \mathcal{C} \neq \emptyset\} \quad , \quad d_\mathcal{C} = \sup\{\alpha \in \mathbb{R} : S^\alpha \cap \mathcal{C} \neq \emptyset\}$$

The collection of such pairs, where \mathcal{C} runs over all maximal chains, is the persistence diagram for the persistence homology of the filtered complex \mathcal{K} .

Persistent cohomology behaves similarly. Indeed, any basis for $H_n(K_\alpha; \mathbb{F})$ yields a well-defined isomorphism $H_n(K_\alpha; \mathbb{F}) \cong H_n(K_\alpha; \mathbb{F})^*$ with the linear dual space, and the latter is naturally isomorphic to $H^n(K_\alpha; \mathbb{F})$, by the universal coefficient theorem. Hence, these isomorphisms turn the S^α 's into a collection of compatible bases for the cohomology groups $H^n(K_\alpha; \mathbb{F})$, showing that persistent homology and cohomology yield the same persistence diagrams.

2.3.1 Persistent Homology of Sliding Window Embeddings

As mentioned in the introduction, there are numerous examples in the literature of persistent homology on sliding window point clouds. For any periodic time series $(x(t) = x(t + kT), k \in \mathbb{Z})$, a sliding window embedding yields a topological loop, and there is a point of high persistence in the persistence diagram for PH_1 [31]. However, the authors of [31] also show, surprisingly, that sliding window embeddings of functions like $x(t) = \cos(t) + a \cos(2t)$ can lie on the boundary of an embedded Möbius strip [31]. We use this to help intuitively explain the time series we obtain for the projective plane (Example 3.4) and the Klein Bottle (Section 5.2). Note that this also means that field coefficients other than \mathbb{Z}_2 are needed to maximize the maximum persistence in PH_1 . In general, for $\cos(t) + a \cos(kt)$, coefficients which are not prime factors of k are needed [31, 38]. Finally, there are works which utilize both PH_1 and PH_2 to quantify the presence of quasiperiodicity in time series data, by estimating the toroidality of a sliding window point cloud [27, 39]. In this work, we extend this suite of examples beyond (possibly twisted) loops and torii to other manifolds.

2.4 Eilenberg-MacLane Coordinates

Though persistent homology is informative, one can further utilize it to perform nonlinear dimensionality reduction on sliding window point clouds, for visualization purposes and reconstruction of the underlying dynamics. To this end, we use “Eilenberg-MacLane coordinates”, [8, 26, 29] which yield maps from point clouds to the circle, and (real or complex) projective spaces. We present next a more detailed summary; maps to the projective plane are particularly interesting, as they allow us to “untwist” non-orientable manifolds like the Klein bottle.

More formally, if G is an abelian group and n is a positive integer, then it is possible to construct a connected CW complex $K(G, n)$, called an Eilenberg-MacLane space, whose homotopy type is uniquely determined by two properties:

1. its j -th homotopy group $\pi_j(K(G, n))$ is trivial for all $j \neq n$
2. $\pi_n(K(G, n)) \cong G$

The Brown representability theorem (for CW complexes and singular cohomology) contends that if B is a CW complex, then there is a natural bijection

$$H^n(B; G) \cong [B, K(G, n)] \tag{2}$$

between the n -th cohomology of B with coefficients in G , and the set of homotopy classes of maps from B to $K(G, n)$.

The two Eilenberg-MacLane spaces we use to generate circular and projective coordinates are: $K(\mathbb{Z}, 1) \simeq S^1$, and $K(\mathbb{Z}/2, 1) \simeq \mathbb{R}\mathbb{P}^\infty = \mathbb{R}^\infty \setminus \{\mathbf{0}\} / \sim$, respectively. Here \mathbb{R}^∞ is the collection of infinite sequences of real numbers $\mathbf{x} = (x_0, x_1, \dots)$ which are nonzero for all but finitely many x_j 's, and $\mathbf{x} \sim \mathbf{y}$ if and only if $\mathbf{x} = r\mathbf{y}$ for some $r \in \mathbb{R} \setminus \{0\}$. One can also regard \mathbb{R}^∞ as the direct limit of the system $\mathbb{R} \subset \mathbb{R}^2 \subset \mathbb{R}^3 \subset \dots$, where the inclusion $\mathbb{R}^j \hookrightarrow \mathbb{R}^{j+1}$ sends (x_0, \dots, x_{j-1}) to $(x_0, \dots, x_{j-1}, 0)$. With this interpretation in mind, $\mathbb{R}\mathbb{P}^\infty$ can be regarded as the direct limit of the system $\mathbb{R}\mathbb{P}^0 \subset \mathbb{R}\mathbb{P}^1 \subset \mathbb{R}\mathbb{P}^2 \subset \dots$, where $\mathbb{R}\mathbb{P}^n = \mathbb{R}^{n+1} \setminus \{\mathbf{0}\} / \sim$. Recently [29], it has been shown that if L is a finite subset of a metric space (\mathbb{M}, \mathbf{d}) , and for $\ell \in L$ we let $B_\alpha(\ell)$ be the open ball of radius α centered at ℓ , then persistent cohomology classes in $PH^1(\mathcal{R}(L); \mathbb{Z}/2)$ can be used to define projective coordinates

$$f_\mu : \bigcup_{\ell \in L} B_\alpha(\ell) \longrightarrow \mathbb{R}\mathbb{P}^n$$

Similarly, persistent cohomology classes in $PH^1(\mathcal{R}(L); \mathbb{Z}/q)$, for appropriate choices of prime $q > 2$, yield circular coordinates [26]

$$f_{\theta, \tau} : \bigcup_{\ell \in L} B_\alpha(\ell) \longrightarrow S^1$$

In both cases, the resulting coordinates mimic the properties of the bijection (2) from Brown's representability.

2.4.1 Projective Coordinates

Here is a sketch of the construction of projective coordinates from persistent cohomology classes. Let $L = \{\ell_0, \dots, \ell_n\} \subset \mathbb{M}$, and fix a cocycle $\mu = \{\mu_{jk}^\alpha\} \in Z^1(R_{2\alpha}(L); \mathbb{Z}/2)$ so that its cohomology class is not in the kernel of the homomorphism

$$i^{2\alpha, \alpha} : H^1(R_{2\alpha}(L); \mathbb{Z}/2) \longrightarrow H^1(R_\alpha(L); \mathbb{Z}/2)$$

induced by the inclusion $R_\alpha(L) \subset R_{2\alpha}(L)$. Since $R_\alpha(L) \subset \check{C}_\alpha(L) \subset R_{2\alpha}(L)$, then the rightmost inclusion yields a nonzero class in $H^1(\check{C}_\alpha(L); \mathbb{Z}/2)$. We let

$$\begin{aligned} f_\mu : \bigcup_{\ell \in L} B_\alpha(\ell) = L^{(\alpha)} &\longrightarrow \mathbb{R}\mathbf{P}^n \\ B_\alpha(\ell_j) \ni b &\mapsto \left[(-1)^{\mu_{j0}^\alpha} |\alpha - \mathbf{d}(b, \ell_0)|_+ : \dots : (-1)^{\mu_{jn}^\alpha} |\alpha - \mathbf{d}(b, \ell_n)|_+ \right] \end{aligned}$$

where $[x_0 : \dots : x_n] \in \mathbb{R}\mathbf{P}^n$ denotes the equivalence class of $(x_0, \dots, x_n) \in \mathbb{R}^{n+1} \setminus \{\mathbf{0}\}$, and $|r|_+ := \max\{0, r\}$ for $r \in \mathbb{R}$. Since $\{\mu_{jk}^\alpha\}$ is a cocycle, it readily follows that the point $f_\mu(b) \in \mathbb{R}\mathbf{P}^n$ is independent of the index $j \in \{0, \dots, n\}$ for which $b \in B_\alpha(\ell_j)$. In other words, f_μ is well defined.

If $\{\nu_{jk}^\alpha\} \in Z^1(R_{2\alpha}(L); \mathbb{Z}/2)$ is cohomologous to $\{\mu_{jk}^\alpha\}$, and $f_\nu : L^{(\alpha)} \longrightarrow \mathbb{R}\mathbf{P}^n$ is the associated map, then $f_\mu \simeq f_\nu$ and hence we get a well defined function

$$\begin{aligned} H^1(R_{2\alpha}(L); \mathbb{Z}/2) &\longrightarrow [L^{(\alpha)}, \mathbb{R}\mathbf{P}^n] \\ [\mu] &\mapsto [f_\mu] \end{aligned}$$

The metric properties of f_μ are also determined by the cohomology class of μ . For if

$$\mathbf{d}_g(\mathbf{x}, \mathbf{y}) := \arccos \left(\frac{|\langle \mathbf{x}, \mathbf{y} \rangle|}{\|\mathbf{x}\| \cdot \|\mathbf{y}\|} \right)$$

denotes the geodesic distance in $\mathbb{R}\mathbf{P}^n$, then it readily follows that

$$\mathbf{d}_g(f_\nu(b), f_\nu(b')) = \mathbf{d}_g(f_\mu(b), f_\mu(b'))$$

for all $b, b' \in L^{(\alpha)}$.

Given a finite set $P \subset L^{(\alpha)}$, taking its image through f_μ yields a new point cloud $f_\mu(P) \subset \mathbb{R}\mathbf{P}^n$. A dimensionality-reduction scheme in $\mathbb{R}\mathbf{P}^n$, referred to as principal projective component analysis, is also defined in [29]. This procedure yields a sequence of maps

$$P_k : f_\mu(P) \longrightarrow \mathbb{R}\mathbf{P}^k, \quad k = 0, \dots, n$$

minimizing an appropriate notion of (metric) distortion. In particular, $P_k \circ f_\mu(P)$ and $P_k \circ f_\nu(P)$ are isometric if μ and ν are cohomologous. The point clouds $P_k \circ f_\mu(P) \subset \mathbb{R}\mathbf{P}^k$ are referred to as the projective coordinates of P , induced by the landmarks $L \subset \mathbb{M}$ and the cohomology class $[\mu] \in H^1(R_{2\alpha}(L); \mathbb{Z}/2)$.

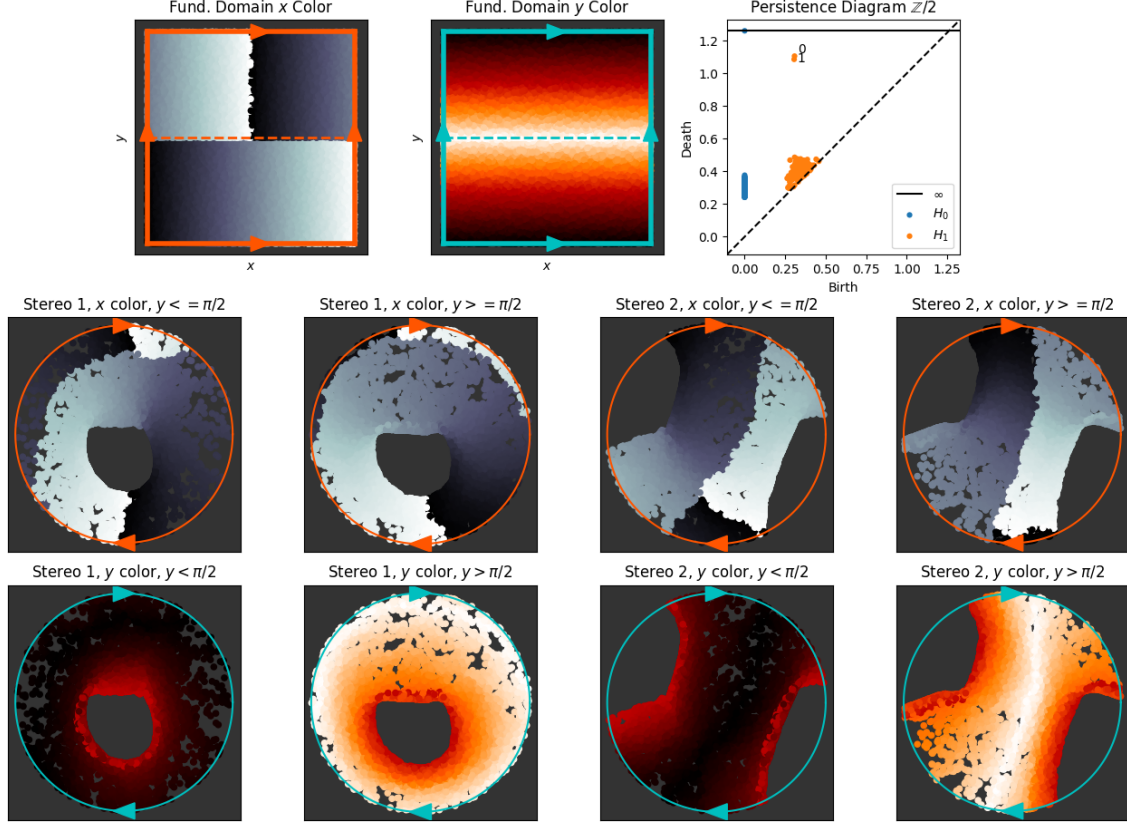


Figure 2: An example of projective coordinates for point sampled from a flat Klein bottle obtained as a quotient of the torus via $[x, y] \sim [x + \pi, -y]$. The two coordinates are colored according to their x and y positions on the fundamental domain $[0, 2\pi] \times [0, \pi]$, and we show two different stereographic projections to the plane from $\mathbb{R}\mathbb{P}^2$. If the fundamental domain is split into distinct parts $A = [0, 2\pi] \times [0, \pi/2]$ and $B = [0, 2\pi] \times [\pi/2, \pi]$, then A and B map to two distinct Möbius strips which are attached at their boundaries at $y = \pi/2$ (medium red for the y colors), which is indeed what happens when the Klein bottle is cut down the middle.

As an example, Figure 2 shows the projective coordinates onto $\mathbb{R}\mathbb{P}^2$ of points sampled from a Klein bottle \mathbb{K} , using the flat metric on the torus \mathbb{T} , descended onto the automorphism $\kappa : (x, y) \mapsto (x + \pi, -y)$. We use the cocycle representative which is the sum of the representative cocycles from the two most persistent classes.

In fact, this is a 2 to 1 map, as shown in Figure 2. Just as a torus can be obtained from gluing two annuli together at their boundary, the Klein bottle can be obtained by gluing two Möbius strips at their boundary. Each one of these Möbius strips is visible in the odd and even columns of the bottom two rows of Figure 2, respectively. In particular, the loops $[0, 2\pi] \times 0$ and $[0, 2\pi] \times \pi$ are at the center of each Möbius strip, and the boundaries of each Möbius strip at $[0, 2\pi] \times \pi/2$ get identified at the center of the projective coordinates plot. We will observe similar projective coordinates for the sliding window of our Klein bottle time series in Section 5.2.

2.4.2 Circular Coordinates

The idea of using the bijection $H^1(B; \mathbb{Z}) \cong [B, S^1]$ to construct circle-valued functions for data, from persistent cohomology classes, was first introduced by de Silva et. al. [8]. Their construction has

shortcomings (not sparse, not transductive) which are addressed in [26]; the latter is the procedure we use in the paper and the one we describe next.

Let $q > 2$ be a prime so that the homomorphism

$$H^1(R_{2\alpha}(L); \mathbb{Z}) \longrightarrow H^1(R_{2\alpha}(L); \mathbb{Z}/q)$$

induced by the projection $\mathbb{Z} \longrightarrow \mathbb{Z}/q$, is surjective. Hence, given $\mu \in Z^1(R_{2\alpha}(L); \mathbb{Z}/q)$ it can be lifted to $\tilde{\mu} \in Z^1(R_{2\alpha}(L); \mathbb{Z})$, and if $\iota : \mathbb{Z} \hookrightarrow \mathbb{R}$ is the inclusion homomorphism, then there are cochains $\theta \in Z^1(R_{2\alpha}(L); \mathbb{R})$ and $\tau \in C^0(R_{2\alpha}(L); \mathbb{R})$ so that θ is the unique harmonic cocycle representative of $\iota^*([\tilde{\mu}])$ and $\iota^\#(\tilde{\mu}) = \theta - \delta^0 \tau$. From this data we define

$$f_{\theta, \tau} : \bigcup_{\ell \in L} B_\alpha(\ell) \longrightarrow S^1 \subset \mathbb{C}$$

$$B_\alpha(\ell_j) \ni b \mapsto \exp \left\{ 2\pi i \left(\tau_j + \sum_{k=0}^n \theta_{jk} \varphi_k(b) \right) \right\}$$

where

$$\varphi_k(b) = \frac{|\alpha - \mathbf{d}(b, \ell_k)|_+}{\sum_{r=0}^n |\alpha - \mathbf{d}(b, \ell_r)|_+}$$

Figure 3 shows an example of this algorithm on a point cloud sampled from a torus, using 400 landmarks. In this example, the algorithm is able to find maps from the points to the inner and outer circle of the torus.

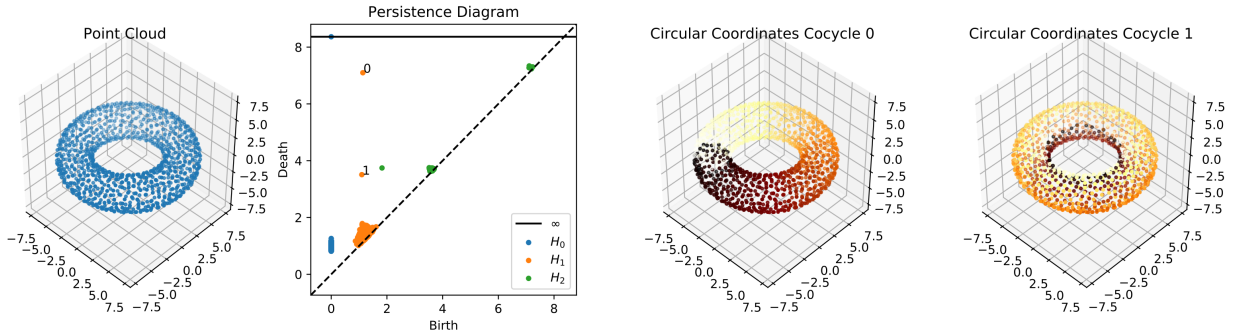


Figure 3: An example of the circular coordinates algorithm on a point cloud sampled from a torus in \mathbb{R}^3 . The third plot shows the coordinates resulting from the representative cocycle of the largest persistence class, which goes around the large circle on the outside, while the fourth plot shows the circular coordinates resulting from the cocycle from the second largest persistence class, which wraps around the inner circle.

3 Preliminary Examples: Distance To A Point As Observation Function

To motivate a more general development of good observation functions on manifolds, we first explore a very specific genre of observation functions: those which arise as the distance to a specified point in the manifold. We then verify the geometric integrity of a delay coordinate mapping of the resulting time series using persistent homology and Eilenberg-Maclane coordinates on a few

examples. Through these tools and a visual comparison of the time series to known examples, we will already be able to explain quite a lot, though a full development of the theory in Section 4 is needed to justify these choices of observation functions.

Example 3.1. *Flat torus \mathbb{T}*

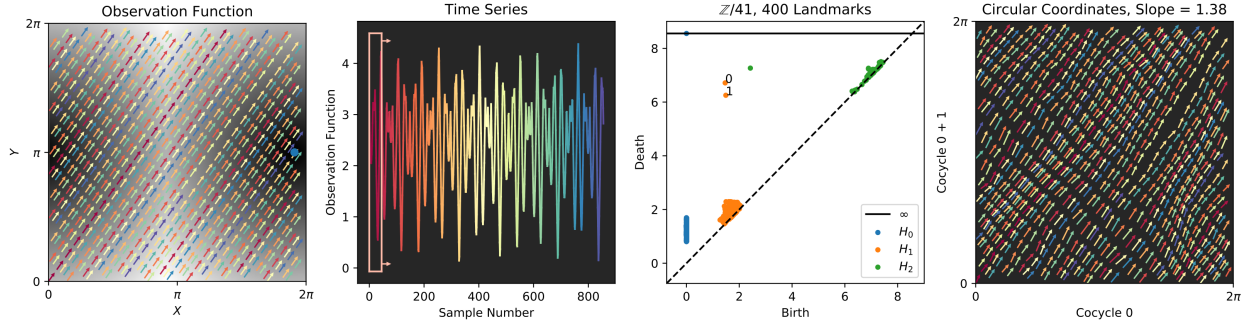


Figure 4: An irrational winding on the flat torus, with an observation function as the distance to the point $(6, \pi)$, which is shown as a blue dot on the left plot. The distance from this point is indicated in gray (dark means close, light means far). The resulting time series is shown in the second plot, with a sliding window indicated with a red box. The third and fourth figures show, respectively, the persistence diagrams of the sliding window point cloud and the resulting circular coordinates. The arrows in the fourth plot are the recovered dynamics; they indicate the order on the sliding windows inherited from the time series. Colors are coordinated between the first, second, and fourth plots. Similar plotting conventions are present in Figures 5, 6, 7, 8, 9.

We first examine the planar torus $\mathbb{T} = \mathbb{R}^2/2\pi\mathbb{Z}^2$ with irrational winding $\gamma(t) = (\sqrt{2}t, t)$ and observation measuring the geodesic distance from the point $(6, \pi)$, which is shown in Figure 4. After performing a delay embedding with window length of 30 samples, we see two persistent $H1$ classes and 1 persistent $H2$ class, which is the signature of a torus. Furthermore, circular coordinates resulting from the top two persistent classes in $H1$ recovered the full original flow specification.

Example 3.2. *Flat Klein Bottle \mathbb{K}*

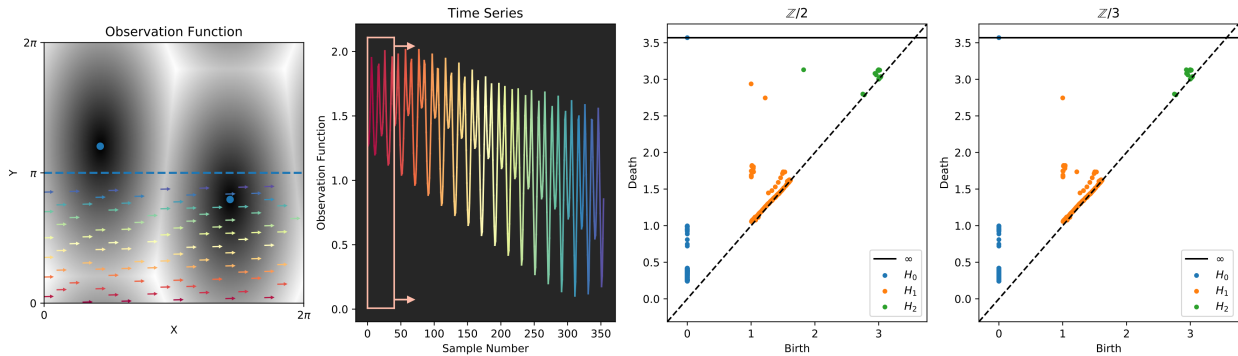


Figure 5: A winding with a very shallow slope on the fundamental domain of a flat Klein bottle, which is double covered by the flat torus by the automorphism $(x, y) \sim (x + \pi, -y)$. The observation function is then a scaled L2 distance from the point $(4.5, 2.5)$, which descends under the automorphism.

As in our projective coordinates example in Figure 2, we now form a quotient on the domain of the flat torus to create a Klein bottle, via the automorphism $\kappa : (x, y) \sim (x + \pi, -y)$. Then, the metric on the torus descends to the Klein bottle via κ . For technical reasons, we use a slightly modified weighted $L2$ flat metric as our distance measure for the observation function; that is

$$d((x_1, y_1), (x_2, y_2)) = \sqrt{\alpha^2(x_1 - x_2)^2 + \beta^2(y_1 - y_2)^2} \quad (3)$$

In this particular example, we let $\alpha = 1$ and $\beta = 0.5$. Finally, we use a flow with a very shallow slope, $(x(t), y(t)) = (t, 0.05t)$, in the fundamental domain $y < \pi$. After performing a sliding window embedding with a window length of 30 samples, we see two persistent classes in $H1$ and one persistent class in $H2$ with $\mathbb{Z}/2$ coefficients, but we only see one class in $H1$ and no classes in $H2$ with $\mathbb{Z}/3$ coefficients. This is indeed the signature of a Klein bottle. We will show projective coordinates on a similar example with a slightly different observation function in Section 5.2, and we will explain more intuitively visual features of the time series at that point.

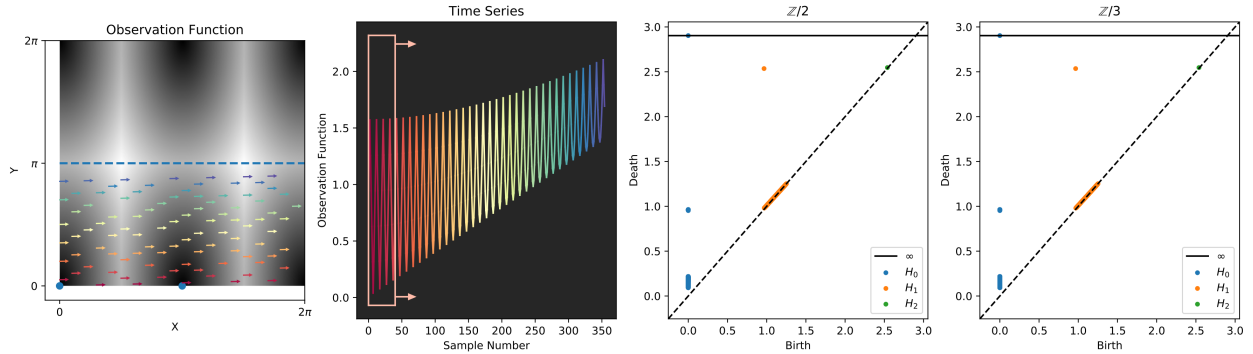


Figure 6: Not all distance functions on the Klein bottle work. The conditions here are the same as in Figure 5, but the point from which distance is measured has been moved to $(\pi, 0)$. The sliding window embedding degenerates to a cylinder in this example.

Note that not every distance function will lead to a reconstruction of the Klein bottle. For instance, if we use an observation function which is a distance to the point $(\pi, 0)$, as in Figure 6, then the sliding window embedding of the resulting time series degenerates to a cylinder. This motivates the injectivity condition in Theorem 4.1.

Example 3.3. Sphere S^2

We now reconstruct the sphere from a given trajectory and distance function. Tralie [37] showed empirically that a sliding window embedding of the helical trajectory $(\theta(t), \varphi(t)) = (t, -\pi/2 + \alpha t)$, under the observation function on the sphere which is the arclength from a point not on the equator or north/south poles, yields an embedding of the sphere. We repeat this here in Figure 7. In this example, simple linear dimension reduction via PCA is able to recover the most of the geometry of the sliding window point cloud, though spherical coordinates are also possible in the Eilenberg-MacLane framework [29].

One pitfall in this example is that the observation point cannot lie on the equator or the north or south poles. In these cases, the helix structure is flattened to a spiral, so the sliding window embedding degenerates to a disc. This motivates the “derivative rank” condition in Theorem 4.1.

Example 3.4. Projective plane \mathbb{RP}^2

We can extend the scheme that we used in Example 3.3 to the projective plane \mathbb{RP}^2 by taking a flow only on the upper hemisphere and performing the antipodal identification at the equator

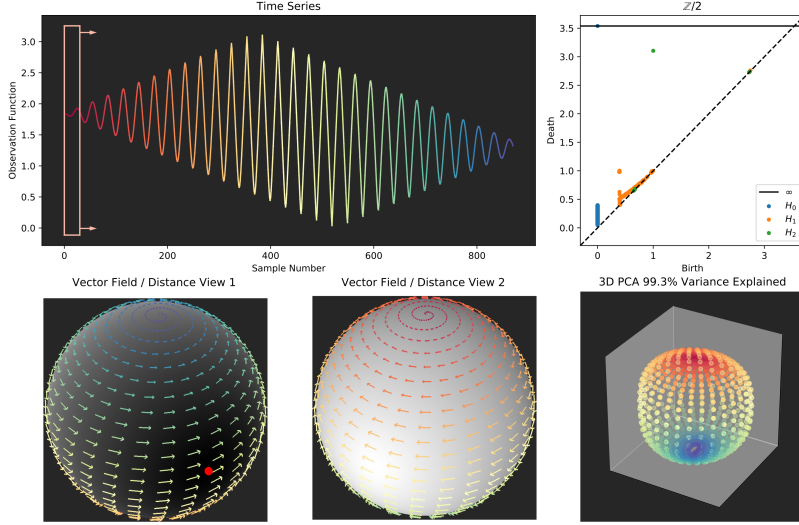


Figure 7: An observation function on the sphere which is the geodesic distance from a point drawn in red. The top and bottom views of the vector field are drawn in the left two figures. 3D PCA of the sliding window embedding, which retains nearly all of the variance of the sliding window point cloud, is shown in the bottom right plot.

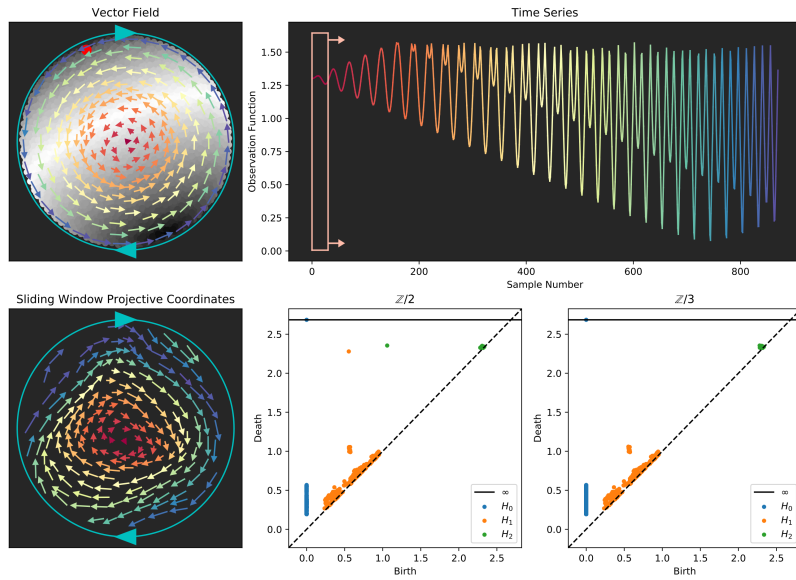


Figure 8: An observation function on the \mathbb{RP}^2 which is the geodesic distance from a point drawn in red.

$x \sim -x$. Figure 8 shows this result, in which a single highly persistent point is present for both H_1 and H_2 using $\mathbb{Z}/2$ coefficients, but in which none are present for $\mathbb{Z}/3$, which is a correct signature of \mathbb{RP}^2 . Interestingly, the quotient identification is visible in the time series itself; the time series in Figure 8 can be obtained from the time series in Figure 7 by reflecting values above the line $y = \pi/2$ across that line. This is because the maximum distance between any two points on \mathbb{RP}^2 is $\pi/2$. Additionally, both the sphere time series and the Möbius loop time series ($\cos(t) + a \cos(2t)$)

are visible in Figure 8. The time series starts off in a spiral, which fills out a disc, and this disc transitions to a spiraling Möbius loop time series which fills out the strip. This visually reflects the fact that $\mathbb{R}P^2$ is the connected sum of a disc and the boundary of a cross-cap. We will use a similar intuition to explain the Klein bottle time series in Section 5.2.

Example 3.5. Genus 2 surface $\mathbb{T}\#\mathbb{T}$

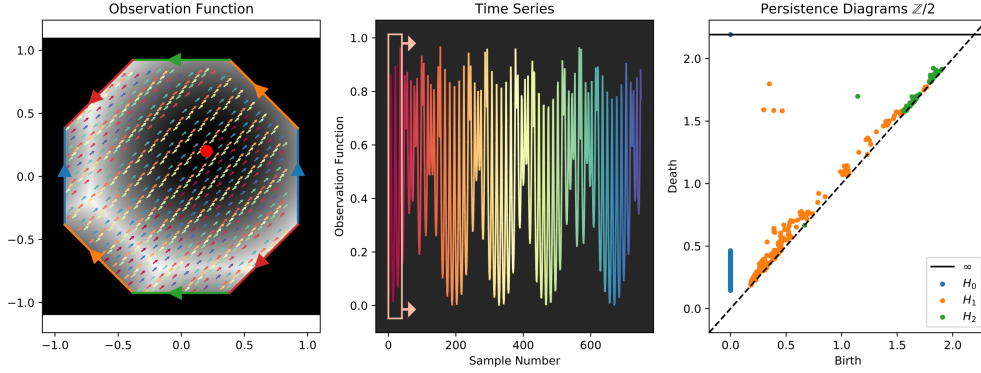


Figure 9: An example of a time series resulting from a dense flow on the 2-holed torus, using the flat squared Euclidean distance [41] from an observation point (shown as a red dot).

Finally, we show a time series whose sliding window embedding lies on the two holed torus. We use an irrational flow with slope $(dt, dt\sqrt{3}/2)$, with an observation function as the squared flat metric on the fundamental domain [41] represented by an octagon with opposite sides identified. Figure 9 shows the result, in which four highly persistent dots are visible in $H1$ and a single persistent dot is visible in $H2$, matching what is expected of the homology of a genus 2 surface.

4 Main Theorem: Characterizing Good Observation Functions

As our main theoretical contribution, we now state more general conditions for good observation functions. Let M be a compact manifold of dimension m , $G : M \rightarrow \mathbb{R}$ a smooth function, and X a vector field with flow ψ_t . Applying G to an integral curve $\gamma_p(t) = \psi_t(p)$ through a point p yields a real-valued function

$$g_p := G \circ \gamma_p$$

in t , the *observation curve* of p . For sufficiently nice G and X , one can recover the point p from a finite uniform sampling of g_p . More precisely, the *Takens map* $\Psi_\tau^N : M \rightarrow \mathbb{R}^{N+1}$ defined by

$$\Psi_\tau^N(p) = (g_p(0), g_p(\tau), g_p(2\tau), \dots, g_p(N\tau))$$

is an embedding for some dimension $N > 0$ and flow time $\tau > 0$. For such G and X we say G is a *good observation* for X .

4.1 Motivation for the approach

As a simple example, take $M = S^1 = \mathbb{R}/2\pi\mathbb{Z}$, $\psi_t(x) = x + t$, and $G(x) = \cos(x)$. The point x is uniquely determined by sampling the two values $g_x(0) = \cos(x)$ and $g_x(\pi/2) = -\sin(x)$ and the Takens map

$$\Psi_{\pi/2}^1(x) = (\cos(x), -\sin(x))$$

is an embedding, so G is a good observation.

On the other hand, the doubly periodic function $G(x) = \cos(2x)$ is not a good observation function. Indeed, any integral curve $g_x(t)$ is invariant under a π -shift of x , as G cannot distinguish between any flow of x and $x + \pi$. In fact, the good observation functions on S^1 for the rotational dynamic are precisely ones with minimum period 2π

In higher dimensions the task of recovering p from g_p becomes less clear. Consider the torus $\mathbb{T} = S^1 \times S^1$ and $G : \mathbb{T} \rightarrow \mathbb{R}$ given by

$$G(x, y) = \cos(x) + \cos(y)$$

and ψ_t an irrational flow

$$\psi_t(x, y) = (x + \alpha t, y + \beta t)$$

and thus for $p = (x, y) \in \mathbb{T}$ we have the observation curve

$$g_p(t) = \cos(x + \alpha t) + \cos(y + \beta t)$$

For G to be good, there must be a τ such that each p is uniquely determined by sampling G along the integral curve γ_p at finitely many τ -steps. Since we are free to shrink τ and increase N , it is natural to examine infinitesimal changes of G along the flow ψ_t . The derivatives

$$\begin{aligned} g_p(0) &= \cos(x) + \cos(y) \\ g'_p(0) &= -\alpha \sin(x) - \beta \sin(y) \\ g_p^{(2)}(0) &= -\alpha^2 \cos(x) - \beta^2 \cos(y) \\ g_p^{(3)}(0) &= \alpha^3 \sin(x) + \beta^3 \sin(y) \end{aligned}$$

up to 3rd order yield the linear equation

$$\begin{pmatrix} 1 & 1 & 0 & 0 \\ -\alpha^2 & -\beta^2 & 0 & 0 \\ 0 & 0 & -\alpha & -\beta \\ 0 & 0 & \alpha^3 & \beta^3 \end{pmatrix} \begin{pmatrix} \cos(x) \\ \cos(y) \\ \sin(x) \\ \sin(y) \end{pmatrix} = \begin{pmatrix} g_p(0) \\ g'_p(0) \\ g_p^{(2)}(0) \\ g_p^{(3)}(0) \end{pmatrix}$$

Equivalently, over \mathbb{C} , the linear system

$$\begin{pmatrix} 1 & 1 & 1 & 1 \\ i\alpha & -i\alpha & i\beta & -i\beta \\ -\alpha^2 & -\alpha^2 & -\beta^2 & -\beta^2 \\ -i\alpha^3 & i\alpha^3 & -i\beta^3 & i\beta^3 \end{pmatrix} \begin{pmatrix} e^{ix} \\ e^{-ix} \\ e^{iy} \\ e^{-iy} \end{pmatrix} = \begin{pmatrix} g_p(0) \\ g'_p(0) \\ g_p^{(2)}(0) \\ g_p^{(3)}(0) \end{pmatrix}$$

has invertible Vandermonde matrix and one can solve for e^{ix} and e^{iy} . Therefore (x, y) is uniquely determined by $g_p^{(k)}(0)$'s. Choosing τ small enough so that $g_p(\tau)$ is close to the 3rd order Taylor polynomial of g_p about 0, we see that p is uniquely determined (modulo 2π) by a τ -uniform finite sampling of g_p .

4.2 Main theorem and proof

The above calculation illustrates our approach to determining whether G is good: by studying the Taylor coefficients $g_p^{(k)}$. Note that $g_p^{(k)}(t)$ is the k -fold derivation of X applied to G at $\psi_t(p)$, i.e., in Lie derivative notation,

$$g_p^{(k)}(t) = \mathcal{L}_X^k G(\psi_t(p)).$$

\mathcal{L}_X is the linear operator on tensor fields which measures infinitesimal change along X , i.e. if T is a tensor then

$$\mathcal{L}_X T(p) = \left. \frac{d}{dt} \right|_{t=0} ((\psi_{-t})_* T_{\psi_t(p)})$$

Writing dG for the differential of G , and \wedge for exterior product, we now state the main result:

Theorem 4.1. *The Takens map Ψ_τ^N is an embedding for some $N > 0$ and flow time $\tau > 0$, if the following conditions hold:*

1. *For any point of $p \in M$ there is an m -tuple $J \in \mathbb{Z}_{\geq 0}^m$ of nonnegative integers such that the m -form*

$$\mathcal{L}_X^{\wedge J} dG := \bigwedge_{j \in J} \mathcal{L}_X^j dG$$

is nonzero at some point on the integral curve $\gamma_p(s)$.

2. *For any pair of distinct points $p, q \in M$ the observation curves $g_p(s)$ and $g_q(s)$ are not identical.*

Proof. For Ψ_τ^N to be an immersion, the cotangent vectors

$$dG|_p, d(G \circ \psi_\tau)|_p, d(G \circ \psi_{2\tau})|_p, \dots, d(G \circ \psi_{N\tau})|_p$$

must span an m -dimensional space. Equivalently, for any point $p \in M$ there must be a strictly increasing m -tuple $I = (i_1, i_2, \dots, i_m) \in \mathbb{Z}_{\geq 0}^m$ of indices such that the determinant m -form $\bigwedge d(G \circ \psi_{i_k \tau})$ does not vanish at p , i.e.

$$\omega_p^I(\tau) := \bigwedge_{i_k \in I} d(G \circ \psi_{i_k \tau})|_p \neq 0$$

The idea is to perform a convolution of the Taylor series of the cotangent curves $d(G \circ \psi_{i_k t})$ and to use condition 1 above to choose sufficiently small τ so that $\omega_p^I(\tau) \neq 0$ for some I . By compactness one makes a uniform choice of small τ so that Ψ_τ is immersive and each observation curve is distinguished on some integer multiple of τ , thereby making Ψ_τ^N injective.

Let $s \geq 0$ be a time parameter for p such that

$$\mathcal{L}_X^{\wedge J} dG$$

is nonzero at $\gamma_p(s)$. Write $\tilde{p} = \gamma_p(s)$ and \mathcal{J}_k for the set of all strictly increasing m -tuples $J = (j_1, j_2, \dots, j_m)$ with degree

$$j_1 + j_2 + \dots + j_m = k$$

satisfying

$$\mathcal{L}_X^{\wedge J} dG|_{\tilde{p}} \neq 0$$

Fix $n > 0$ to be the minimal integer for which \mathcal{J}_n is nonempty (possible by condition 1 above).

Let $A(t)$ be the m by n matrix with (k, j) th entry

$$A_{k,j}(t) = \frac{i_k^j (t-s)^j}{j!}$$

and $L : T_{\bar{p}}M \rightarrow \mathbb{R}^n$ the linear map given by $\mathcal{L}_X^j dG|_{\bar{p}}$ in the j^{th} coordinate. So the k^{th} component of the composition $A(t) \circ L$ yields the n^{th} order Taylor polynomial about $t = s$ of the cotangent curve $d(G \circ \psi_{i_k t})|_p$.

By Cauchy-Binet formula applied to $A(t)$ and L , the top exterior product

$$\omega_p^I(t) = \bigwedge_{i_k \in I} d(G \circ \psi_{i_k t})|_p$$

has n^{th} order Taylor series expansion about $t = s$ with n^{th} coefficient

$$C_n = \frac{\det(V)}{a_n} \sum_{J \in \mathcal{J}_n} |I^J| \cdot \mathcal{L}_X^{\wedge J} dG|_{\bar{p}}$$

where

- a_n is a nonzero constant depending only on n
- $|I^J| = \prod i_k^{j_k - k + 1}$

and

$$\det(V) = \prod_{k < k'} (i_{k'} - i_k) \neq 0$$

is the nonzero determinant of the $m \times m$ Vandermonde matrix V with $(k, j)^{\text{th}}$ entry

$$V_{k,j} = i_k^{j-1}$$

where we take $0^0 = 1$.

By the minimality assumption on \mathcal{J}_n , all the lower degree Taylor coefficients

$$C_j = 0 \text{ for } j < n$$

are zero. So the Taylor expansion of $\omega_p^I(t)$ has the form

$$\omega_p^I(t) = (t - s)^n C_n + R_p^n(t)$$

where $R_p^n(t)$ is the n^{th} order Taylor error term with vanishing limit

$$\lim_{t \rightarrow s} \frac{R_p^n(t)}{(t - s)^n} = 0$$

We show C_n is nonzero for suitable choice of I . For $\tilde{J} \in \mathcal{J}_n$ the colexigraphically maximal element of \mathcal{J}_n , choose I so that

$$|I^J| \ll |I^{\tilde{J}}|$$

for all $J < \tilde{J}$ and thus

$$\sum_{J \in \mathcal{J}_n} |I^J| \cdot \mathcal{L}_X^{\wedge J} dG|_{\bar{p}} \neq 0.$$

This can be done by making some of the rightmost coordinates of I large. So the n^{th} Taylor coefficient

$$C_n \neq 0$$

is nonzero. Hence we may choose a time $\eta > s$ sufficiently close to s so that the Taylor error $R_p^n(\eta)$ is small and the inequality

$$\omega_q^I(\eta) \neq 0$$

holds for all q in a neighborhood of p , and this property remains invariant under shrinking η closer to s . By compactness of M there is a finite collection of triples (I_r, η_r, s_r) such that the collection of m -forms

$$\{\omega^{I_r}(\eta_r)\}$$

do not all vanish at any given point of M and the cotangent vectors

$$\{d(G \circ \psi_{i_k \eta_r})|_q\}_{i_k \in I_r}$$

specified by I_r are linearly independent. Choose $\tau > 0$ small enough so that there is an integer multiple of τ lying in the interval (s_r, η_r) for each r . Then the Takens map Ψ_τ^N is an immersion for all $N > 0$ bounding I_r and η_r/τ .

So Ψ_τ^N is locally injective and the difference map

$$\Psi_\tau^N(p) - \Psi_\tau^N(q)$$

does not vanish for all $p \neq q$ in an open neighborhood U of the diagonal in $M \times M$, and this property is invariant under scaling $N \mapsto Nd$ and $\tau \mapsto \tau/d$ for an integer $d > 0$ (with U fixed).

For distinct $(p, q) \in M \times M \setminus U$, we may shrink τ so that g_p and g_q are distinguished on some integer multiple of τ and $\Psi_\tau(p) \neq \Psi_\tau(q)$. By compactness of $M \times M \setminus U$, there is a uniform choice of τ and N making Ψ_τ^N injective, hence an embedding. □

5 An Application to Surfaces via Fourier theory

Now that we have our theory in hand, we can examine another class of observation functions which are constructed from Fourier modes, in addition to our distance-based observation functions in Section 3.

5.1 The Torus

We start by characterizing all smooth observations $G : \mathbb{T} \rightarrow \mathbb{R}$ for a vector field X of irrational flow

$$\psi_t(x, y) = (x + \alpha t, y + \beta t)$$

yielding toroidal delay embedding. For G write the Fourier expansion

$$G(x, y) = \sum_{(n, m) \in \mathbb{Z}^2} \hat{G}(n, m) \cdot \exp(i(nx + my))$$

where $\hat{G}(n, m) \in \mathbb{C}$ is the $(n, m)^{\text{th}}$ Fourier coefficient of G . Set

$$\text{Supp } \hat{G} = \{(n, m) \in \mathbb{Z}^2 \mid \hat{G}(n, m) \neq 0\}$$

the *support* of \hat{G} .

Theorem 5.1. *A smooth function $G : \mathbb{T} \rightarrow \mathbb{R}$ is a good observation for an irrational winding if and only if the support $\text{Supp } \hat{G}$ of the Fourier coefficients generates \mathbb{Z}^2 as an abelian group.*

Proof. Write $e_{n,m} = \exp(i(nx + my))$ for the $(n, m)^{\text{th}}$ Fourier basis element. The k -fold Lie derivative $\mathcal{L}_X^k G$ has Fourier coefficient

$$\widehat{\mathcal{L}_X^k G}(n, m) = i^k (n\alpha + m\beta)^k \cdot \hat{G}(n, m)$$

and thus Fourier expansion

$$\mathcal{L}_X^k G = \sum_{(n,m) \in \mathbb{Z}^2} i^k (n\alpha + m\beta)^k \hat{G}(n, m) \cdot e_{n,m}$$

Since α/β is irrational, the coefficients

$$c_{n,m} = i \cdot (n\alpha + m\beta)$$

are nonvanishing and pairwise distinct. Therefore the Vandermonde matrix with $(n, m) \times j^{\text{th}}$ entry

$$(c_{n,m}^k)$$

is nonsingular and the projection

$$G * e_{n,m} = \hat{G}(n, m) \cdot \exp(i(nx + my))$$

can be written as an infinite sum

$$\hat{G}(n, m) \cdot \exp(i(nx + my)) = \sum_{j=0}^{\infty} b_j \mathcal{L}_X^j G \quad (4)$$

Hence the values of $\mathcal{L}_X^k G$ on a point $(u, v) \in \mathbb{T}$ uniquely determine

$$\hat{G}(n, m) \cdot e^{i(nu + mv)}$$

If $\text{Supp } \hat{G}$ generates \mathbb{Z}^2 , then there is some finite product

$$\prod_{(n_j, m_j) \in \text{Supp } \hat{G}} e^{i(n_j u + m_j v)} = e^{iu}$$

and thus u , and similarly v , are uniquely determined modulo 2π by the observation curve $G \circ \gamma_{u,v}$ and condition 2 of Theorem 4.1 above is satisfied.

If $d\mathcal{L}_X^j G \wedge d\mathcal{L}_X^k G$ vanishes at p for all $j, k \geq 0$, then by equation 4 above, the 2-form

$$d(G * e_{n,m}) \wedge d(G * e_{n',m'}) = \det \begin{pmatrix} n & m \\ n' & m' \end{pmatrix} \hat{G}(n, m) \hat{G}(n', m') \cdot e_{n,m} e_{n',m'}$$

also vanishes at p for all pairs $(n, m), (n', m') \in \mathbb{Z}^2$. Thus

$$\det \begin{pmatrix} n & m \\ n' & m' \end{pmatrix} = 0 \text{ for all } (n, m), (n', m') \in \text{Supp } \hat{G}$$

and $\text{Supp } \hat{G}$ cannot generate \mathbb{Z}^2 . So condition 1 of Theorem 4.1 is satisfied if $\text{Supp } \hat{G}$ generates \mathbb{Z}^2 .

Conversely, suppose $\text{Supp } \hat{G}$ does not generate \mathbb{Z}^2 . By the classification of finitely generated abelian groups, there is a \mathbb{Z} -basis

$$(n_1, m_1), (n_2, m_2)$$

for \mathbb{Z}^2 such that $\text{Supp } \hat{G}$ is generated by

$$a \cdot (n_1, m_1), b \cdot (n_2, m_2)$$

where a and b are integers not both ± 1 . Then there is some $(u, v) \notin 2\pi\mathbb{Z}^2$ such that

$$\begin{pmatrix} an_1 & am_1 \\ bn_2 & bm_2 \end{pmatrix} \cdot \begin{pmatrix} u \\ v \end{pmatrix}$$

takes values in $2\pi\mathbb{Z}$, so that $\exp(i(nu + mv)) = 1$ for all $(n, m) \in \text{Supp } \hat{G}$. So for any point $(x, y) \in \mathbb{T}$, $(x + u, y + v) \in \mathbb{T}$ is a distinct point with the same observation curve, and no Takens map can distinguish between (x, y) and $(x + u, y + v)$. \square

Remark 5.2. *For the irrational winding on the torus, the Koopman eigenfunctions are given by the Fourier basis. The Vandermonde inversion in equation (4) above shows that the Fourier modes of an observation are determined by its delay mapping. We are not aware of such a connection between Takens and Koopman, though it seems natural in this context.*

By Theorem 5.1, whether or not G is good for an irrational flow depends only on the support $\text{Supp } \hat{G}$. The quasiperiodic function

$$g(t) = \cos \sqrt{2}t + \cos t \tag{5}$$

is the observation of $G(x, y) = \cos(x) + \cos(y)$ along the irrational flow $(\sqrt{2}t, t)$ on the planar torus $\mathbb{T} = \mathbb{R}^2/2\pi\mathbb{Z}^2$. A point cloud densely sampled from the sliding window $\text{SW}_1^{10} g(t)$ coordinates given by 10 uniform shifts of $g(t)$ yields a curve in \mathbb{R}^{10} with toroidal persistence.

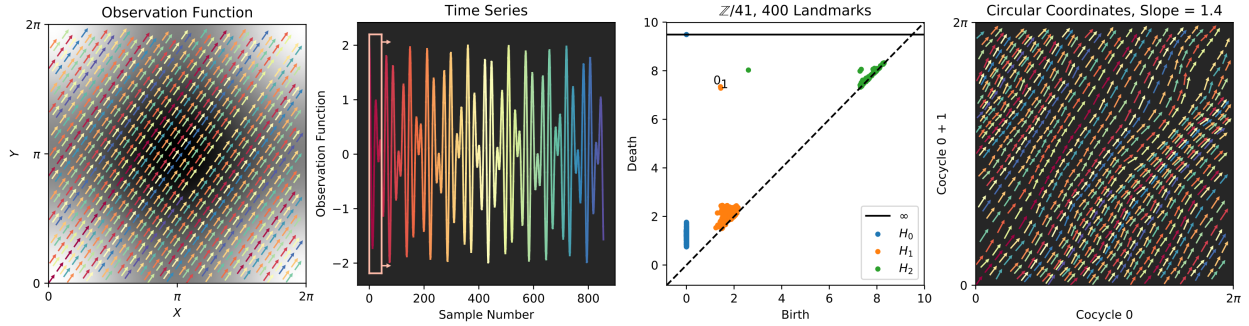


Figure 10: The observation function $\cos(x) + \cos(y)$ for the same flow as Figure 4

5.2 The Klein bottle

As in our example in Section 2.4.1, we write the Klein bottle \mathbb{K} as the quotient of the torus \mathbb{T} by the automorphism $\kappa : (x, y) \mapsto (x + \pi, -y)$. The irrational flow on the \mathbb{T} is not κ -invariant since κ is orientation reversing in the y coordinate. To approximate the shallow flow in Figures 5 and 6 above, we construct a vector field which flows cyclically along a repeller $y = 0$ and an attractor $y = \pi$ by restricting a linear flow to the fundamental domain $[0, 2\pi] \times [0, \pi]$ and flatten it out on the boundary circles $y = 0, \pi$. For $\alpha, \beta \in \mathbb{R}$ with $0 < \alpha/\beta \ll 1$ irrational, let X_ϵ be a vector field on the rectangle given by

$$X_\epsilon(x, y) = \begin{cases} (\alpha, \rho(y)) & 0 \leq y \leq \epsilon \\ (\alpha, \beta) & \epsilon < y \leq \pi - \epsilon \\ (\alpha, \rho(\pi + \epsilon - y)) & \pi - \epsilon < y \leq \pi \end{cases}$$

where ρ is a smooth function on a neighborhood of $[0, \epsilon]$ with $\rho(0) = 0$, $\rho(\epsilon) = \beta$ making X_ϵ smooth. For example, $\rho = \beta \exp(1/(y/\epsilon - 1)^2 - 1)$. Then X_ϵ extends uniquely to a κ -invariant vector field on \mathbb{T} , and therefore induces a vector field on \mathbb{K} .

Theorem 5.3. *Let $G : \mathbb{T} \rightarrow \mathbb{R}$ be a κ -invariant function on \mathbb{T} . For fixed $N\tau$, the Takens map*

$$\Psi_\tau^N : \mathbb{K} \rightarrow \mathbb{R}$$

induced by G and X_ϵ for arbitrarily small ϵ and slope $\alpha/\beta \ll 1$ is an embedding if and only if the following conditions hold:

1. $G(x, \pi)$ and $G(x, 0)$ have period π in x and do not differ by of a shift
2. $\text{Supp } \hat{G}$ generates \mathbb{Z}^2

Proof. Suppose G is good for X_ϵ . Since X_ϵ flows horizontally at $y = 0, \pi$, condition 1) must hold so that each point is uniquely determined by its observation curve. Condition 2) must hold as well, since X_ϵ is given by an irrational winding away from the ϵ -neighborhood of $y = 0, \pi$ and the same argument as in Theorem 5.1 above applies for sufficiently shallow slope α/β because $N\tau$ is fixed.

Conversely, suppose conditions 1) and 2) hold. X_ϵ is given by an irrational flow away from the ϵ -neighborhood of $y = 0, \pi$. Furthermore, any point in the ϵ -strip with $y \neq 0, \pi$ may be flowed to a point where X_ϵ has irrational slope. The same argument as in Theorem 5.1 shows that the Takens map restricts to an embedding on $y \neq 0, \pi$.

By condition 1, the observation curve of a point (x, y) where $y = 0, \pi$ uniquely determines x modulo π , and is periodic and therefore distinct from any observation curve for $y \neq 0, \pi$. So each point is uniquely determined by its observation curve as per condition 2) of Theorem 4.1.

It remains to show that the Takens map is immersive at $y = 0, \pi$. If not, then $\frac{\partial G}{\partial y}$ vanishes on the circles $y = 0, \pi$, a neighborhood about which Ψ_τ^N would fail to immerse, a contradiction. \square

According to Theorem 5.3, the “simplest” κ -symmetric good observation is

$$G(x, y) = \cos 2x + \cos x \sin y + \cos y. \quad (6)$$

Indeed, the Fourier coefficients of G are supported at $(\pm 2, 0), (\pm 1, \pm 1), (0, \pm 1)$, which generates \mathbb{Z}^2 . Along the limit cycles we have $G(x, 0) = \cos 2x + 1$ and $G(x, \pi) = \cos 2x - 1$, which are distinct and doubly periodic.

Intuitively, the $\cos 2x$ term is responsible for delay-mapping the limit cycles $y = 0, \pi$ via a double covering. Without this term, the boundary $G(x, 0) = 1$, $G(x, \pi) = -1$ along the bottom and top boundaries, respectively. Not only are these boundaries no longer identified, but they also each map to a single point, turning the Klein bottle into a sphere. The delay mapping of $\cos x \sin y$ fills two Möbius strips in conjunction with $\cos(2x)$, while the $\cos(y)$ term serves to “separate” the Möbius strips, as shown in the right hand side of Figure 5.2.

We can also see this by parameterizing the flow by a single variable $t = x$ and examining the time series directly. In this case, the time series is

$$g(t) = \cos(2t) + \cos(t) \sin\left(\frac{\alpha}{\beta}t\right) + \sin\left(\frac{\alpha}{\beta}t\right) \quad (7)$$

for $\epsilon < \frac{\alpha}{\beta}t < \pi - \epsilon$. Over small ranges of t , the sine terms are approximately constant. The time series is then of the form $\cos(2t) + a \cos(t)$, $|a| < 1$; that is, its sliding window embedding locally parameterizes the boundary of a Möbius strip [31]. As it moves further along, a changes, and so it fills out the strip.

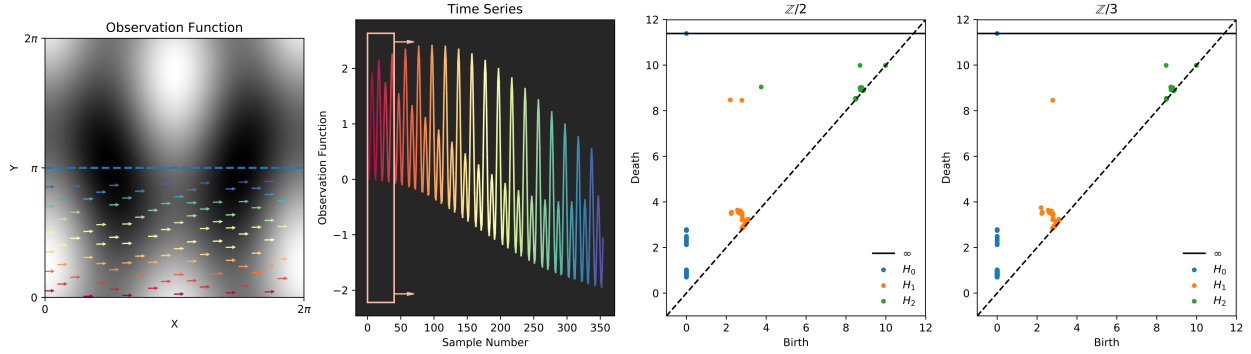


Figure 11: The observation function from Equation 6 for the same flow as Figure 5

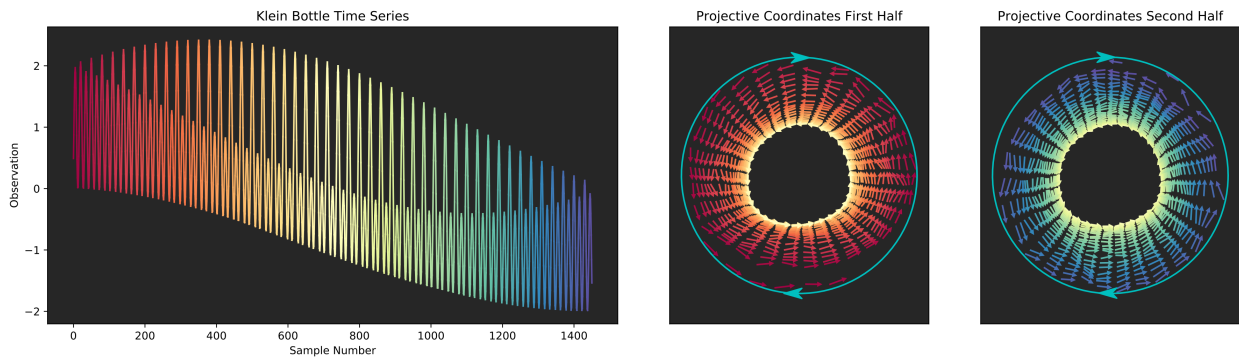


Figure 12: Projective coordinates for a Klein bottle with observation function specified in Equation 6. We plot the first half in the second subplot, which traces a Möbius strip from its core to its boundary, shown in yellow. Then, that boundary is glued to a second Möbius strip, which corresponds to the second half of the time series, as shown on the right.

6 Discussion

It is clear what circular and toroidal observations look like in the time domain, and as we have mentioned, there are many applications that take advantage of this knowledge. The theory developed in this paper has enabled us to develop examples of signals recovering other manifolds. With such a database of signals, we can begin to train our eyes to recognize other underlying manifolds in naturally occurring time series. Moreover, just like circular and toroidal sliding window embeddings have interpretations in terms of physical phenomena, the presence of klein bottles, mobius strips, spheres, projective planes, etc, should also have practical meaning. It is unlikely that one could identify said time series in the wild without such examples in hand. Finally, we note that not only do we have a method for producing time series recovering other manifolds, which we have validated empirically using persistent homology and Eilenberg MacClane coordinates, but the method is backed by a theorem that indicates exactly when it will succeed/fail.

References

- [1] Hassan Arbabi. Introduction to koopman operator theory of dynamical systems. 2018.

- [2] Ulrich Bauer. Ripser: a lean c++ code for the computation of vietoris-rips persistence barcodes. *Software available at <https://github.com/Ripser/ripser>*, 2017.
- [3] Juan P Bello. Measuring structural similarity in music. *IEEE Transactions on Audio, Speech, and Language Processing*, 19(7):2013–2025, 2011.
- [4] Elodie F Briefer, Anne-Laure Maigrot, Roi Mandel, Sabrina Briefer Freymond, Iris Bachmann, and Edna Hillmann. Segregation of information about emotional arousal and valence in horse whinnies. *Scientific reports*, 4:9989, 2015.
- [5] Gunnar Carlsson. Topology and data. *Bulletin of the American Mathematical Society*, 46(2):255–308, 2009.
- [6] William Crawley-Boevey. Decomposition of pointwise finite-dimensional persistence modules. *Journal of Algebra and its Applications*, 14(05):1550066, 2015.
- [7] Suddhasattwa Das and Dimitrios Giannakis. Delay-coordinate maps and the spectra of koopman operators. *arXiv preprint [arXiv:1706.08544](https://arxiv.org/abs/1706.08544)*, 2017.
- [8] Vin De Silva, Dmitriy Morozov, and Mikael Vejdemo-Johansson. Persistent cohomology and circular coordinates. *Discrete & Computational Geometry*, 45(4):737–759, 2011.
- [9] Vin de Silva, Primož Skraba, and Mikael Vejdemo-Johansson. Topological analysis of recurrent systems. In *Workshop on Algebraic Topology and Machine Learning, NIPS*, 2012.
- [10] Herbert Edelsbrunner and John Harer. Persistent homology—a survey. *Contemporary mathematics*, 453:257–282, 2008.
- [11] Herbert Edelsbrunner and John Harer. *Computational topology: an introduction*. American Mathematical Soc., 2010.
- [12] Herbert Edelsbrunner and Ernst P Mücke. Three-dimensional alpha shapes. *ACM Transactions on Graphics (TOG)*, 13(1):43–72, 1994.
- [13] Saba Emrani, Harish Chintakunta, and Hamid Krim. Real time detection of harmonic structure: A case for topological signal analysis. In *Acoustics, Speech and Signal Processing (ICASSP), 2014 IEEE International Conference on*, pages 3445–3449. IEEE, 2014.
- [14] Jordan Frank, Shie Mannor, and Doina Precup. Activity and gait recognition with time-delay embeddings. In *AAAI*. Citeseer, 2010.
- [15] Hitesh Garhar and J.A. Perea. Sliding window persistence of quasiperiodic functions. 2018.
- [16] Robert W Ghrist. *Elementary applied topology*. Createspace, 2014.
- [17] Bryan Glaz, Igor Mezić, Maria Fonoberova, and Sophie Loire. Quasi-periodic intermittency in oscillating cylinder flow. *Journal of Fluid Mechanics*, 828:680–707, 2017.
- [18] Allen Hatcher. *Algebraic Topology*. Cambridge University Press, 2002.
- [19] Hanspeter Herzel, David Berry, Ingo R Titze, and Marwa Saleh. Analysis of vocal disorders with methods from nonlinear dynamics. *Journal of Speech, Language, and Hearing Research*, 37(5):1008–1019, 1994.

- [20] Holger Kantz and Thomas Schreiber. *Nonlinear time series analysis*, volume 7. Cambridge university press, 2004.
- [21] Firas A Khasawneh and Elizabeth Munch. Chatter detection in turning using persistent homology. *Mechanical Systems and Signal Processing*, 70:527–541, 2016.
- [22] B. O. Koopman. Hamiltonian systems and transformation in hilbert space. *Proceedings of the National Academy of Sciences*, 17(5):315–318, 1931.
- [23] Igor Mezić. Analysis of fluid flows via spectral properties of the koopman operator.
- [24] Katherine Morrison, Anda Degeratu, Vladimir Itskov, and Carina Curto. Diversity of emergent dynamics in competitive threshold-linear networks: a preliminary report. *arXiv preprint arXiv:1605.04463*, 2016.
- [25] David D Nolte. The tangled tale of phase space. *Physics today*, 63(4):33–38, 2010.
- [26] J.A. Perea. Towards sparse and stable circular coordinates. 2018.
- [27] Jose A Perea. Persistent homology of toroidal sliding window embeddings. In *Acoustics, Speech and Signal Processing (ICASSP), 2016 IEEE International Conference on*, pages 6435–6439. IEEE, 2016.
- [28] Jose A Perea. A brief history of persistence. *arXiv preprint arXiv:1809.03624*, 2018.
- [29] Jose A Perea. Multiscale projective coordinates via persistent cohomology of sparse filtrations. *Discrete & Computational Geometry*, 59(1):175–225, 2018.
- [30] Jose A Perea, Anastasia Deckard, Steve B Haase, and John Harer. Sw1pers: Sliding windows and 1-persistence scoring; discovering periodicity in gene expression time series data. *BMC bioinformatics*, 16(1):257, 2015.
- [31] Jose A Perea and John Harer. Sliding windows and persistence: An application of topological methods to signal analysis. *Foundations of Computational Mathematics*, 15(3):799–838, 2015.
- [32] Emil Plesnik, Olga Malgina, Jurij F Tasic, Saso Tomazic, and Matej Zajc. Detection and delineation of the electrocardiogram qrs-complexes from phase portraits. 2014.
- [33] Joan Serra, Xavier Serra, and Ralph G Andrzejak. Cross recurrence quantification for cover song identification. *New Journal of Physics*, 11(9):093017, 2009.
- [34] Cornelis J Stam. Nonlinear dynamical analysis of eeg and meg: review of an emerging field. *Clinical Neurophysiology*, 116(10):2266–2301, 2005.
- [35] Floris Takens et al. Detecting strange attractors in turbulence. *Lecture notes in mathematics*, 898(1):366–381, 1981.
- [36] Christopher Tralie, Nathaniel Saul, and Rann Barr-On. Ripser.py: A lean persistent homology library for python. *Journal of Open Source Software (JOSS)*, 2018.
- [37] Christopher J Tralie. *Geometric Multimedia Time Series*. Duke ph.d. dissertation, Department of Electrical and Computer Engineering, Duke University, 2017.

- [38] Christopher J Tralie and John Harer. Moebius beats: The twisted spaces of sliding window audio novelty functions with rhythmic subdivisions. In *18th International Society for Music Information Retrieval (ISMIR), Late Breaking Session*, 2017.
- [39] Christopher J. Tralie and Jose A. Perea. (quasi)periodicity quantification in video data, using topology. *SIAM Journal on Imaging Sciences*, 11(2):1049–1077, 2018.
- [40] Vinay Venkataraman, Karthikeyan Natesan Ramamurthy, and Pavan Turaga. Persistent homology of attractors for action recognition. In *Image Processing (ICIP), 2016 IEEE International Conference on*, pages 4150–4154. IEEE, 2016.
- [41] Anton Zorich. Flat surfaces. *Frontiers in number theory, physics, and geometry I*, pages 439–585, 2006.